Beni-Suef University Journal of Basic and Applied Sciences

RESEARCH

Open Access

Green synthesis of silver nanoparticles using dietary antioxidant rutin and its biological contour

Kinjal Kubavat[1], Pooja Trivedi[1], Hafsa Ansari[1], Anita Kongor[2], Manthan Panchal[2,3], Vinod Jain[2] and Gaurang Sindhav[1*]

Abstract

Background: Dietary and wholesome antioxidant rutin is considered advantageous due to its potential protective role for numerous diseases related to oxidative stress, high safety, cost-effectiveness, and extensive biological effects. The present study accounts for an expeditious method for the synthesis of silver nanoparticles (AgNPs) using rutin.

Results: The presence of AgNPs was affirmed by UV–visible spectroscopy at 425 nm, and FESEM and zeta sizer analysis revealed the average size of the AgNPs 80–85 nm and 160 d.nm, respectively. Zeta potential measurements (− 30.3 mV) showed that the AgNPs have reasonably good stability. Element mapping analysis of the AgNPs was confirmed by XRD and AFM, while FTIR spectra of the AgNPs showed the existence of functional groups. In the DPPH assay, highest radical scavenging activity of AgNPs, 86.95 ± 01.60%, was confirmed. The interaction of AgNPs with CT-DNA and HS-DNA was studied spectrophotometrically, and the data display a shift in the respective spectra. Furthermore, interaction with pBR322 DNA, *λ* DNA, CT-DNA, and HS-DNA was deliberated by a nicking assay that shows the physicochemical properties of AgNPs. Antibacterial activity was evaluated by the standard well-diffusion method against *Escherichia coli* and *Staphylococcus aureus,* and cytotoxicity was assessed against human WBCs by MTT assay.

Conclusion: As per this appraisal, it can be concluded that it is a cost-effective, simple, and eco-friendly tactic and such NPs are beneficial to improve therapeutics since the antioxidant, DNA interaction, antibacterial, and cytotoxic exploits offer a new horizon of euthenics.

Keywords: Rutin, Silver nanoparticles (AgNPs), Spectroscopy, DNA, Antibacterial activity, Cytotoxicity

1 Background

Nanotechnology (NT) is an emerging integrative approach because of its burgeoning impacts on a wide range of applications and has pivotal roles in human health too, most notably in medical queries that can offer personalized therapeutics [1]. It is defined as the design, development, and application of materials and devices whose least functional makeup is on a nanometer scale.

Nanoparticles (NPs) evince improved properties due to their physicochemical properties such as shape, size, size distribution, and larger surface area-to-volume ratio [2–4]. NPs are synthesized using different methods and more consistently using chemical methods [5, 6]. However, chemical methods cannot evade the use of toxic chemicals in the synthesis protocol. Hence, the need of the era is to develop a high-yielding, pocket-friendly, and non-toxic modus-operandi. Therefore, the biological approach to the synthesis of NPs becomes vital [7].

Currently, the synthesis of NPs from several noble metals like palladium (Pd), tin (Sn), copper (Cu), silver (Ag), gold (Au), etc., has received more attention because of

*Correspondence: drsindhavlab@gmail.com

[1] Department of Zoology, BMT, HGC and WBC, University School of Sciences, Gujarat University, Ahmedabad, India
Full list of author information is available at the end of the article

their exclusive properties as well as their application in diverse fields. Furthermore, silver nanoparticles (AgNPs) play an important role in therapeutics because they have demonstrated excellent effects in many in vitro biological activities [8].

Curiosity about dietary phenolics has increased, due to their antioxidant properties, and is considered an important nutraceutical in account of many health benefits. Flavonoids are the largest group of naturally occurring phenolic compounds found in fruits and vegetables with significant nutritional and pharmacological values [9]. Because of their adequate structural features, flavonoids are candidates to be employed in the synthesis of AgNPs [10]. A common flavonoid, quercetin, and a naturally occurring plant polyphenol gallic acid were used in the synthesis of AgNPs [11]. Some studies have also conveyed natural reducing agents such as chitosan, starch, and tannic acid for the synthesis of AgNPs and AuNPs [12].

In this study, rutin a sugar-based natural flavonoid (Vitamin P) is employed as a reducing agent in the synthesis of AgNPs. It possesses antioxidant activity and is largely extracted from natural sources such as oranges, lemons, grapes, limes, berries, and peaches. Pharmacological studies have reported the beneficial effects of rutin in many disease conditions [13]. It has anti-inflammatory and anti-carcinogenic properties and is also constructive for chronic venous insufficiency, hypertension, infections, atherosclerosis, osteoarthritis, hemorrhoids, stroke prevention, and high cholesterol [14]. This study would be beneficial to expand our understanding as no detailed study was conducted for AgNPs synthesis using rutin and its biological interaction.

DNA (Deoxyribonucleic acid) is the genetic blueprint of living organisms. An amalgam of genome and NT is an intensive field that embroils the use and the creation of bioinspired materials and their technologies for highly selective biosensing, gene therapy, nanodrugs, nanoarchitecture engineering, and nanoelectronics [15]. Increasing research has been offered to a fundamental understanding of how the interactions between the NPs and DNA molecules could amend DNA and its biochemical activities [16]. However, a worthy long-term goal is to develop a new universal platform, based on NPs–DNA interaction for novel personalized diagnostics and therapeutics [15].

Bacterial septicity is one of the most meditative global health issues. The emergence of bacterial resistance to antibiotics is a major health problem, and therefore, it is critical to develop new antibiotics with a novel mechanism of action to overcome various problems [17]. In recent times, the antibacterial activity of Ag has gained profound magnitude due to increasing bacterial resistance to antibiotics [18]. The AgNPs also possess high surface vicinity which increases the energy and enhances the antimicrobial activity of NPs [19].

Cytotoxicity assays are among the first in vitro bioassays used to predict the toxicity of constituents to various tissues. The safety evaluation of compounds such as drugs, cosmetics, food additives, pesticides, and industrial chemicals is growing year by year. The need for reliable, sensitive, and quantitative assays that enable an analysis of a large number of compounds in preclinical research is therefore increasing [20]. MTT (3-(4,5-dimethylthiazol-2-yl)-2,5-diphenyl-2H-tetrazolium bromide) assay has become the gilt standard for determination of cell viability and proliferation. MTT assay is one of the most commonly used colorimetric assays for measuring the respiratory ability of the mitochondrial succinate-tetrazolium reductase system that reduces yellow MTT to purple color formazan product by NADH. Thus, the MTT assay serves as a quantitative, penetrating, and convenient method for evaluating the cytotoxicity of new compounds.

Keeping the above milieu in view, the present study is intended to research in the field of green chemistry for AgNPs synthesis using rutin. Such particles are well versed in a number of applications related to health. Hence, it is important to explore biological activity, viz. antioxidant, DNA interaction, antibacterial as well as cytotoxicity of biologically synthesized and characterized AgNPs to probe its therapeutic potential.

2 Methods

Silver nitrate ($AgNO_3$), rutin trihydrate ($C_{27}H_{30}O_{16}{\cdot}3H_2O$), HiSep, Trypan Blue, MTT, RPMI-1640, Nutrient agar powder, Luria Bertani broth-miller (*LB Broth*), and Penicillin streptomycin (Pen Strep) were purchased from HiMedia, India. Calf thymus DNA (CT-DNA) was procured from Sigma-Aldrich, USA. Herring sperm DNA (HS-DNA) and DPPH (2,2-Diphenyl-1-picrylhydrazyl) were purchased from SRL, India. pBR322 DNA, λ DNA, and Gentamicin were from Thermo Fisher Scientific, India. All other reagents used in this study were of analytical grade. The solutions used for experiments were prepared in distilled water (DW) (Millipore system), and respective solvents.

2.1 Synthesis of AgNPs

AgNPs were prepared using rutin as a reducing agent, as described by Ajitha et al. [21] with some modification 0.001 M $AgNO_3$ solution in DW was heated for 10 min. at 60 °C, followed by the addition of drop by drop 0.01 M rutin under continuous and stable stirring till the solution becomes yellow to dark brown. The formed AgNPs

were collected by centrifugation at 2000 rpm for 20 min. and dried in a hot air oven at 80 °C.

2.2 Characterization of AgNPs

2.2.1 UV–visible spectroscopy analysis

Primary identification of AgNPs formation was carried out by observing the color change of the reaction solution. The bioreduction of $AgNO_3$ to AgNPs was checked by UV–visible spectrophotometer double beam LI-2800 manufactured by Lasany, and spectrograph of the synthesized AgNPs was recorded using a quartz cuvette with water as a reference at a scanning range of 200–600 nm.

2.2.2 Zeta sizer

Dynamic light scattering (DLS) is a physics practice and can be used to define the size distribution of small particles in the solution. The size and zeta potential of the aliquots of AgNPs were experiential by Zeta sizer Nano ZS90, Malvern instruments in a disposable cell at 25 °C using Zeta sizer 7.13 software after 5 min. of sonication to avoid aggregation of particles.

2.2.3 X-ray diffraction (XRD) analysis

The particle size and nature of the AgNPs were perceived using XRD. This was carried out using PANalytical X'Pert Powder model with 40 mA, 45 kV with Cukα radians at 2θ angle.

2.2.4 Atomic force microscope (AFM) analysis

The particle size distribution and surface morphology of the AgNPs were examined using AFM. AFM images were taken with a MultiMode 8 atomic force microscope 17 with a Nanoscope V controller by Bruker.

2.2.5 Field emission scanning electron microscope (FESEM) analysis

The FESEM is a prevailing technique to obtain magnified images, with a good depth of field for the analysis of individual crystals or any other characteristic morphological features, especially electrically conductive samples. The secondary electrons emitted after the interaction of the electron beam with the sample are detected to produce good quality, high-resolution images which give the topographic information regarding the sample. The size and morphology of AgNPs were studied using NOVA Nano-SEM 450.

2.2.6 Fourier-transform infrared (FTIR) analysis

The dried AgNPs were ground with KBr pellets with the help of KBr press, Model M-15, Technosearch instruments and analyzed by FTIR in the wavenumber frequency ranging from 3500 to 500 cm^{-1} for the functional groups present on it which are responsible for bioreduction of $AgNO_3$. All the dimensions were recorded in transmittance mode using Bruker Alpha, Lab India Instrument Private Limited, functioned by OPUS 7.5 software.

2.3 DPPH radical scavenging activity

DPPH radical scavenging assay for rutin and AgNPs was achieved according to Blois [22]. Briefly, the DPPH solution of 6×10^{-5} M was prepared in methanol, and 500 µl of this solution was added to 500 µl of each sample (10–80 µg/ml). Shake vigorously and allow to stand for 30 min. at room temperature. Methanol/DPPH (1:1) solution was used as a control. All the tubes were in triplicates. Take absorbance at 520 nm against methanol as a blank under EPOCH microplate spectrophotometer by BioTek using Gen5™ software. The scavenging activity was calculated by %inhibition $[(A0 - A1)/\ A0] \times 100$, where A0 is the absorbance of the control and A1 is the absorbance of the sample and the results were expressed as the mean ± SE.

2.4 Spectroscopic studies of DNA, rutin, AgNPs, and their interactions

CT-DNA (50 µg/ml) and HS-DNA (33 µg/ml) were dissolved in DW and stored at 5 °C for 24 h. with occasional stirring to ensure the formation of a homogeneous solution. The final concentration of DNA solutions was determined by spectrophotometer at 260 nm using molar extinction coefficient $\varepsilon 260 = 6600\ cm^{-1}\ M^{-1}$. Spectral changes of CT-DNA and HS-DNA were monitored by a UV–visible spectrophotometer after the addition of 0.1 mM rutin and a colloidal solution of AgNPs [23].

2.5 DNA nicking assay

DNA nicking assay for AgNPs was performed by using agarose gel electrophoresis to evaluate its binding and protective nature to different forms of DNA against free radicals [24]. Various DNA such as pBR322 (double-stranded circular), λ (double-stranded linear), CT (double-stranded linear), and HS (single-stranded linear) were used as aimed DNA. Fenton reagent was prepared by mixing 30 mM H_2O_2 (hydrogen peroxide), 50 µM ascorbic acid, and 80 µM $FeCl_3$ (ferric chloride). DNA was added to 10 µl of AgNPs suspension and incubated at 37 °C for 30 min., 60 min, and 90 min. Then, 10 µl Fenton's reagent was added and again incubated at 37 °C for 30 min., 60 min, and 90 min. After incubation, loading dye was added to the reaction solution and the mixture

was run on 1% agarose gel at 50 V in a TAE buffer. The gel was observed and photographed by the BioDoc-it™ imaging system, UVP after electrophoresis.

2.6 Antibacterial activity

The antibacterial activity of the 0.1 mM rutin and colloidal solution of AgNPs was assessed against Gram-negative as well as Gram-positive strains, namely *Escherichia coli (E. coli)* and *Staphylococcus aureus* (*S. aureus)*, respectively, using pour plate method. Pen-Strep and Gentamicin were used as the positive control, whereas DW and methanol as the negative control [3].

2.7 Cytotoxic assessment using MTT assay

An in vitro inhibitory effect of the biosynthesized AgNPs on human WBCs (White blood cells) was determined by the MTT colorimetric assay [25]. WBCs were separated from the blood given by a healthy volunteer. Trypan Blue dye exclusion method is used to determine the total numbers of WBCs, and cell viability was also calculated. Then, a fixed number of WBCs were taken, i.e., 1×10^5 cells. The WBCs along with RPMI-1640, MTT (ratio between MTT and media was kept at 1:10), and 20 µl AgNPs of different concentrations were added as doses. The tubes were incubated at 37 °C for 4 h. in the presence of 5% CO_2 and then centrifuged at 4000 rpm for 10 min. To the pellet DMSO was added in a volume same as the media, and this leads to the formazan crystals dissolving. All the tubes were placed in triplicates. The absorbance was read at 570 nm using a microplate reader. Then, the %viability of all samples was calculated by the following formula, %viability = (Sample O.D/Control O.D) × 100. The results were expressed as the mean ± SE.

3 Results

3.1 UV–visible spectroscopy analysis

After visible observation of color change, the characterization of the AgNPs using spectroscopy showed

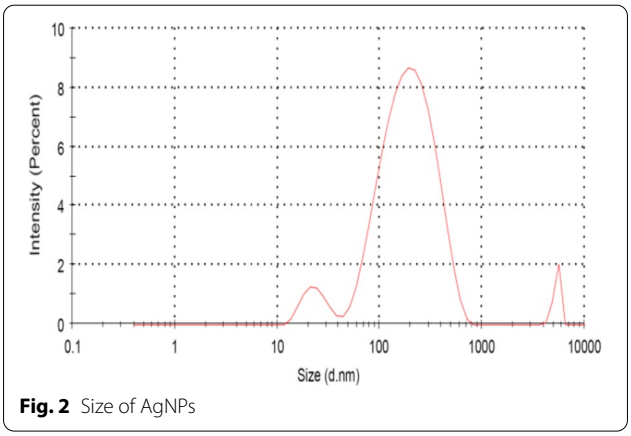

Fig. 2 Size of AgNPs

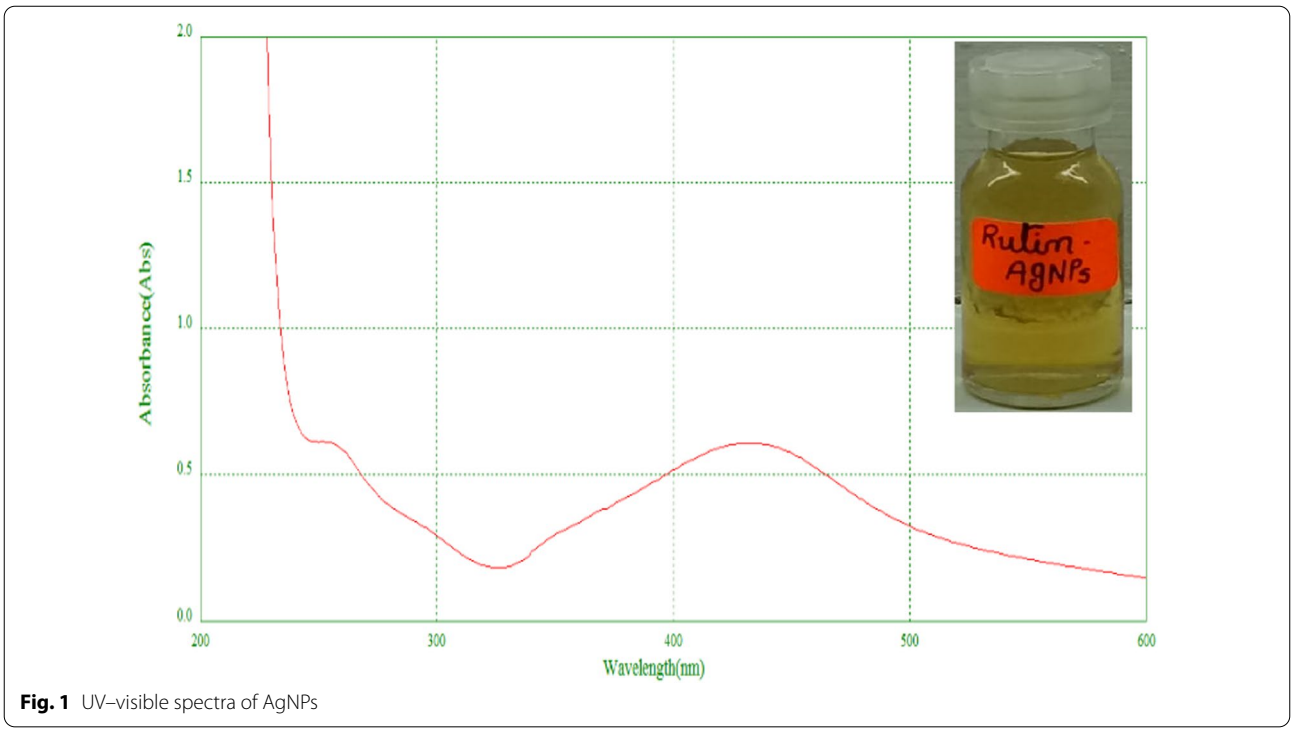

Fig. 1 UV–visible spectra of AgNPs

that the biosynthesis was successful. AgNPs showed an SPR peak at 425 nm (Fig. 1). The frequency and width of the plasmon resonance are due to the shape and size of AgNPs.

3.2 Zeta sizer

As the exact size and charge are imperative fragments of NPs synthesis, the record of particle size distribution was taken with a zeta sizer where 160d.nm was the size found for AgNPs with 0.4 PdI (Fig. 2). The zeta potential of AgNPs was observed at − 30.3 mV which confirms the higher stability of particles (Fig. 3).

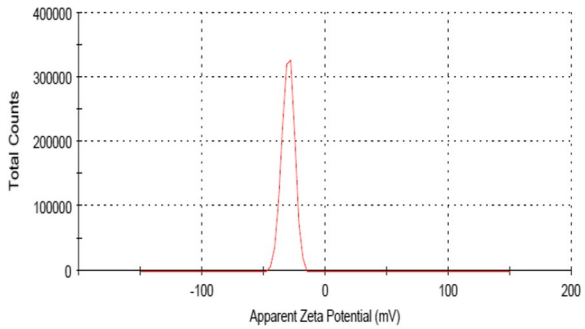

Fig. 3 Zeta potential of AgNPs

3.3 XRD analysis

The XRD pattern showed several Bragg reflections that may be indexed based on the face-centered cubic (FCC) structure of silver. XRD analysis confirmed that the AgNPs were in the form of nanostructures, as evidenced by the peaks at 2θ values of 38.2987°, 44.3396°, 46.3668°, 54.9849°, 64.6043°, 77.5561°, and 81.7470° corresponding to (111), (200), (002), (020), (220), (311), and (222) planes, respectively, which confirm the FCC structure of the formed AgNPs (Fig. 4). These Bragg reflections of silver were in good agreement with the JCPDS file No. 004–0783. It was found that the average size from XRD data and using the Debye–Scherrer equation was approximately 31.10 nm. Besides the above-mentioned peaks, other obtained peaks can be due to rutin. Prakash et al. [26] also observed other peaks of phytochemicals of aqueous leaf extract in reducing, capping, and stabilizing the synthesized AgNPs.

3.4 AFM analysis

AFM was used to analyze particle morphology, viz. shape and size. AFM images of AgNPs show irregular-shaped morphology, and Fig. 5 shows 3D and 2D AFM images of the AgNPs where the size of the particles is found to be 47.29 nm.

3.5 FESEM analysis

Figure 6 shows that most of the AgNPs are spherical and some are irregular. The size is between 80 and 85 nm.

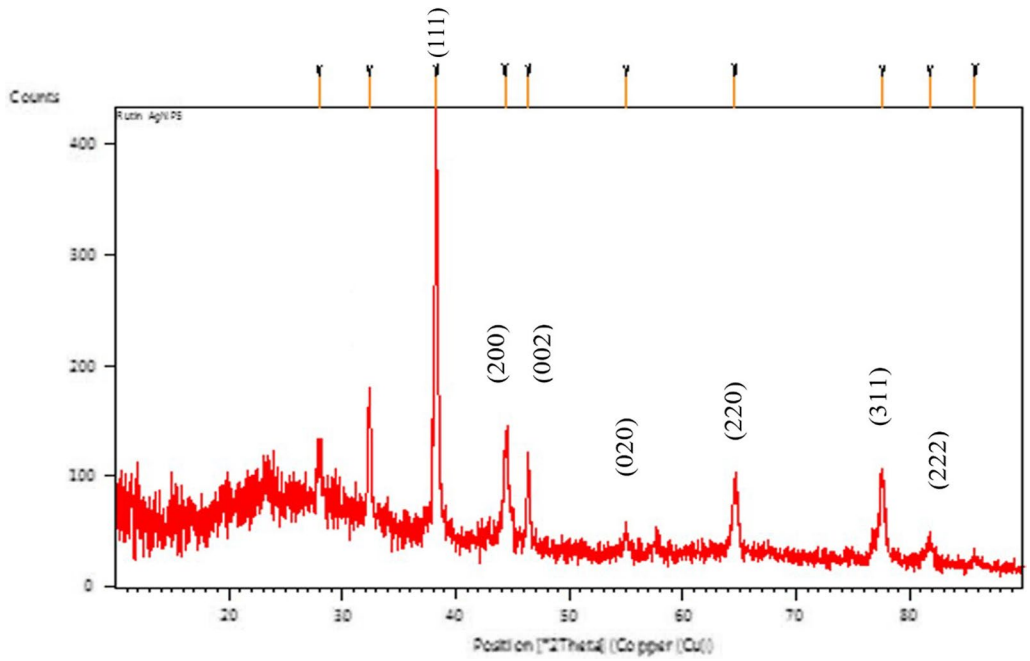

Fig. 4 XRD pattern of AgNPs

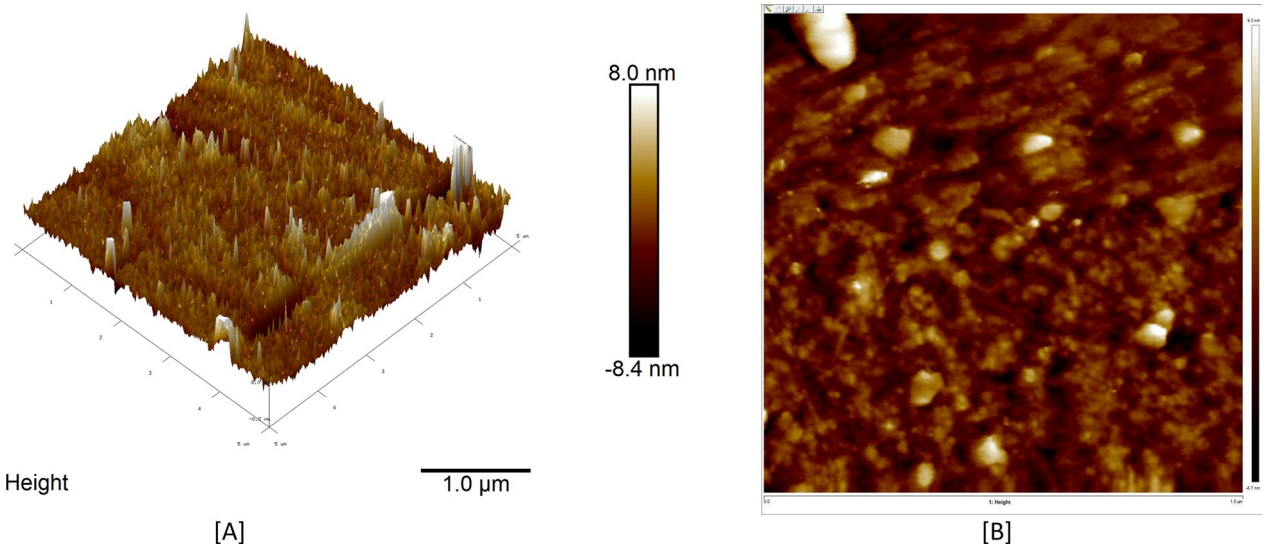

Fig. 5 AFM image of AgNPs. **A** 3D image and **B** 2D image

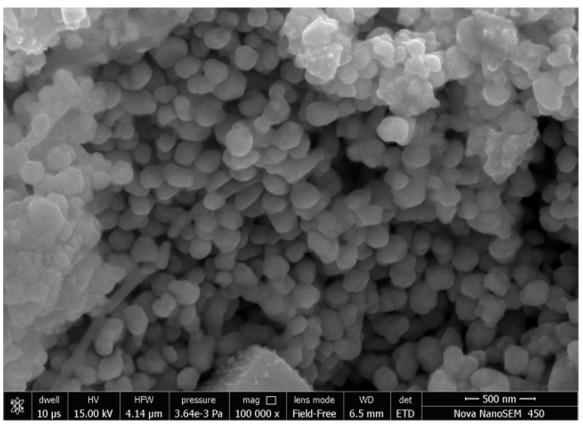

Fig. 6 FESEM image of AgNPs

3.6 FTIR analysis

The FTIR spectrum is shown in Fig. 7. Data of this pragmatic part give 3369.98 cm^{-1} and 3250.92 cm^{-1} (water OH stretch), 2918.80 cm^{-1} and 2850.10 cm^{-1} (alkane C–H medium), 1650.59 cm^{-1} (δ-lactam C=O strong), 1508.65 cm^{-1} (C=O amide strong), 1384.23 cm^{-1} (phenol O–H medium) which are responsible for reduction and capping of AgNPs. In previous study by Hooresfand et al. [27], rutin showed the characteristic peaks in 3285.79, 3400, 3035.80, 1750, 1629.76, and 1602.09 cm^{-1}.

3.7 DPPH radical scavenging activity

The DPPH assay illustrates that along with standard rutin, AgNPs also possess significant antioxidant activity in a concentration-dependent manner. This happens due to diminution by accepting the hydrogen or electron. The outcome of the assay showed effective % inhibition, 86.95 ± 01.60% at 80 µg/ml by AgNPs (Fig. 8).

3.8 Spectroscopic studies of DNA, rutin, AgNPs, and their interactions

This practical part of the study presented that in CT-DNA and HS-DNA hyperchromic effect was observed while interacting with standard rutin (Fig. 9). CT-DNA and HS-DNA were stabilized while interacting with AgNPs, as it has emblematic hypochromic and bathochromic influence (Fig. 10).

3.9 DNA nicking assay

To expand the interactive and protective nature of AgNPs with DNA, in this study various forms of DNA were exposed to AgNPs and Fenton's reagent at 37 °C for 30 min., 60 min., and 90 min. for time-dependent study. The DNA nicking assay assesses the conversion of native DNA to nicked form because of exposure to radicals generated by Fenton's reagent.

In Fig. 11, AgNPs showed no difference in the native form of pBR322 (Lane: 2, 5, 8) at various incubation times while compared with control, lane 1. In pBR322 DNA Fenton's reagent caused a super shift by cleaving the phosphodiester chain, from supercoiled (Form I) to open circular (Form II) and linear (Form III) after 30 min. (Lane: 3), and further incubation of 60 min. and 90 min. displayed more scission with open circular (Form II) and linear (Form III) forms (Lane: 6, 9). Exposure to both Fenton's reagent and AgNPs under similar conditions reports

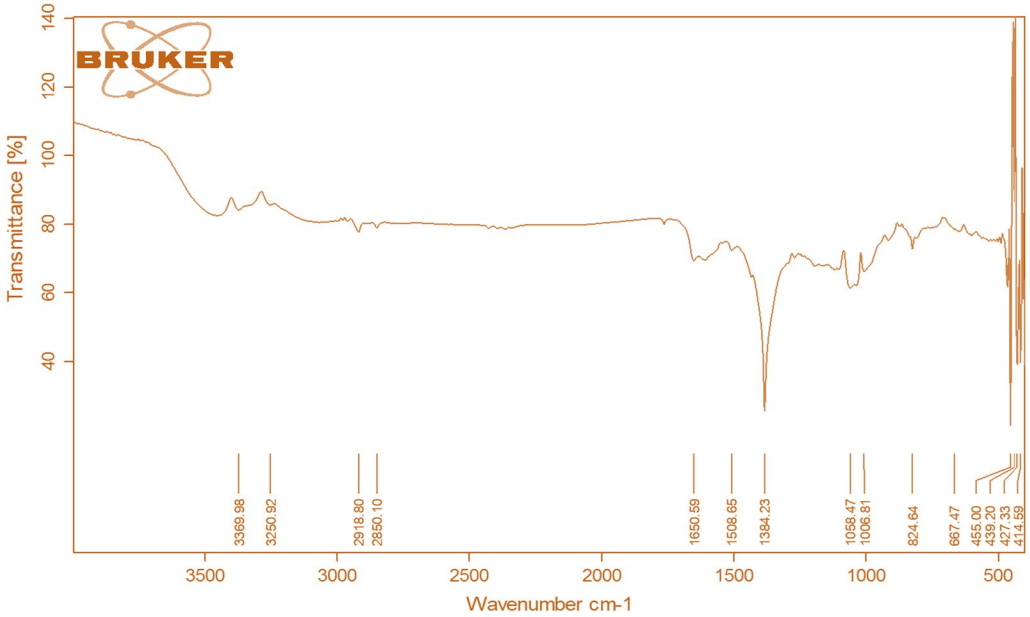

Fig. 7 FTIR spectra of AgNPs

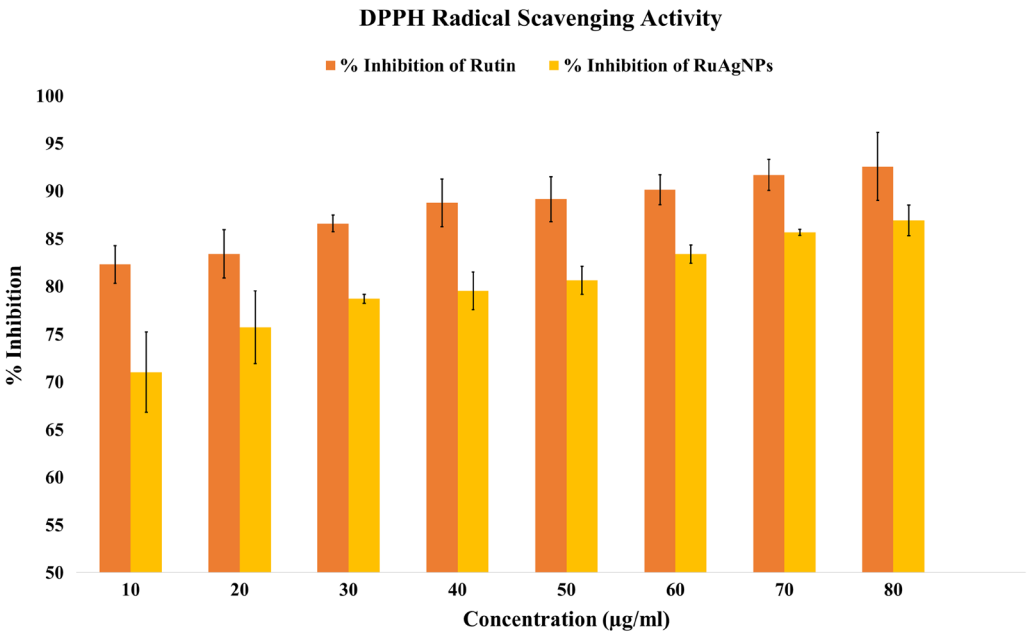

Fig. 8 DPPH radical scavenging activity of rutin and AgNPs

that AgNPs were able to protect DNA from free radicals by conserving Form I and Form II (Lane: 4, 7, 10).

A tailing pattern of λ DNA in Fig. 11 (Lane: 13, 16, 19) stated that DNA was getting cleaved with produced hydroxyl radical and showed more scission in DNA with increasing time. On the other hand, the incubation of AgNPs and DNA did not depict any cleavage (Lane: 12, 15, 18). While DNA was incubated with both Fenton's reagent and AgNPs, DNA was found to be protected which shows the interaction of AgNPs with λ DNA (Lane:

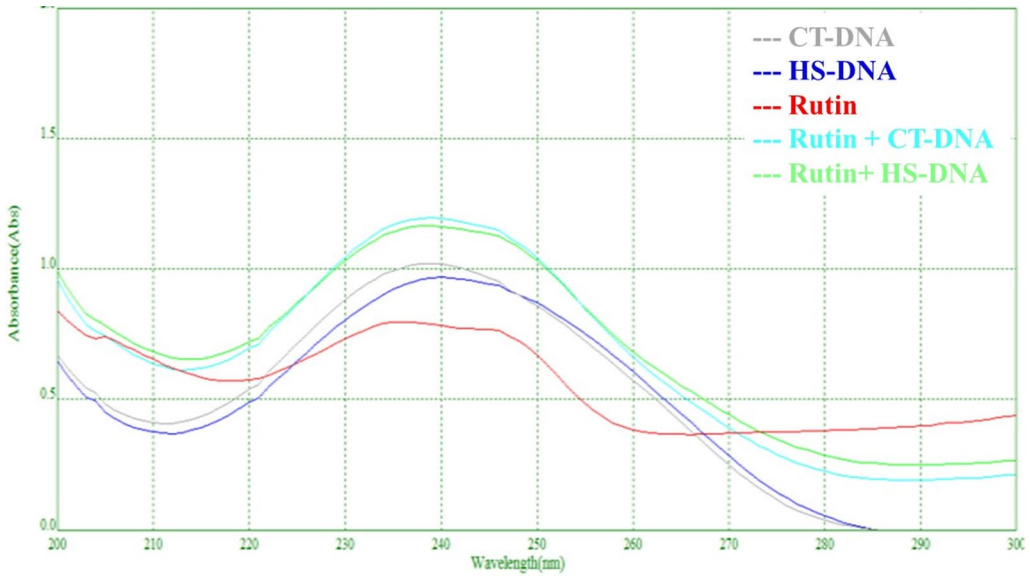

Fig. 9 DNA interaction with rutin

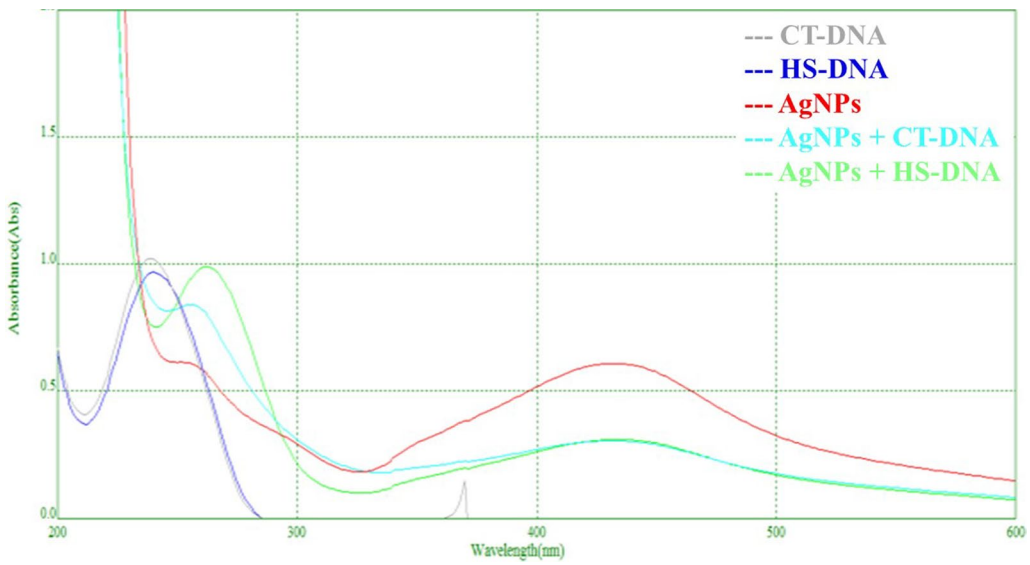

Fig.10 DNA interaction with AgNPs

14, 17, 20). Thus, the present study evidently suggests the protection of pBR322 and λ DNA by the AgNPs.

As per Fig. 12, Fenton's reagent, AgNPs, and a mixture of both have no significant structural effect on CT-DNA and validate no interaction with DNA. Contrary to this, co-incubation of HS-DNA with AgNPs, Fenton's reagent, and a mixture of both, respectively, revealed successive loss in the quantity of DNA. Increasing time of incubation also showed a successive loss in DNA with the above mixture which suggests AgNPs have direct DNA binding/damaging properties.

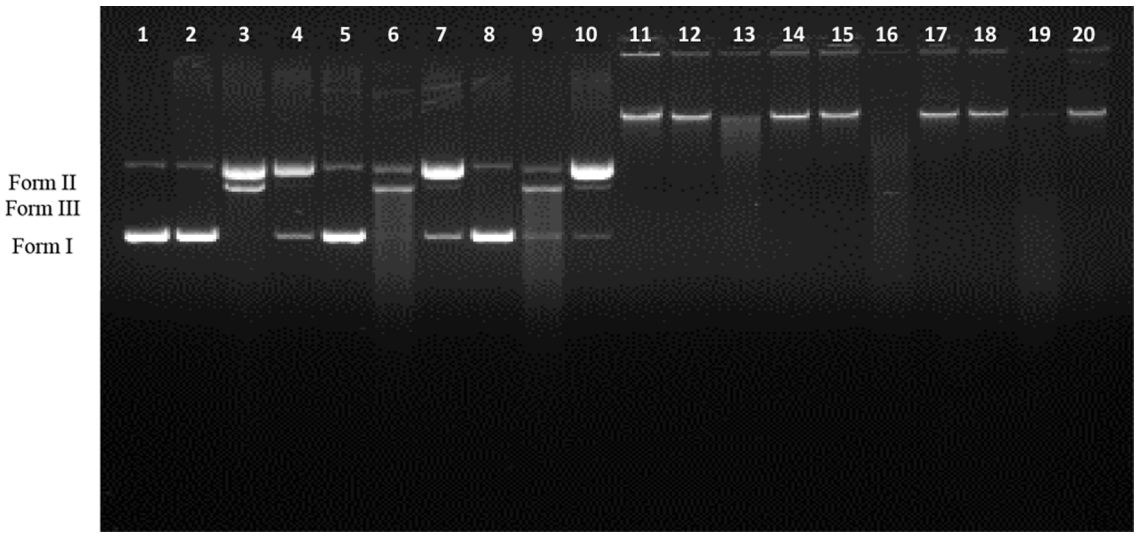

Fig. 11 Interaction of AgNPs with pBR322 DNA and λ DNA. Lane 1 = Control pBR322; Lane 2 = pBR322 + AgNPs (37 °C for 30 min.); Lane 3 = pBR322 + Fenton's reagent (37 °C for 30 min.); Lane 4 = pBR322 + AgNPs ((37 °C for 30 min.)) + Fenton's reagent (37 °C for 30 min.); Lane 5 = pBR322 + AgNPs (37 °C for 60 min.); Lane 6 = pBR322 + Fenton's reagent (37 °C for 60 min.); Lane 7 = pBR322 + AgNPs ((37 °C for 60 min.)) + Fenton's reagent (37 °C for 60 min.); Lane 8 = pBR322 + AgNPs (37 °C for 90 min.); Lane 9 = pBR322 + Fenton's reagent (37 °C for 90 min.); Lane 10 = pBR322 + AgNPs ((37 °C for 90 min.)) + Fenton's reagent (37 °C for 90 min.) Lane 11 = Control λ DNA; Lane 12 = λ DNA + AgNPs (37 °C for 30 min.); Lane 13 = λ DNA + Fenton's reagent (37 °C for 30 min.); Lane 14 = λ DNA + AgNPs ((37 °C for 30 min.)) + Fenton's reagent (37 °C for 30 min.); Lane 15 = λ DNA + AgNPs (37 °C for 60 min.); Lane 16 = λ DNA + Fenton's reagent (37 °C for 60 min.); Lane 17 = λ DNA + AgNPs ((37 °C for 60 min.)) + Fenton's reagent (37 °C for 60 min.); Lane 18 = λ DNA + AgNPs (37 °C for 90 min.); Lane 19 = λ DNA + Fenton's reagent (37 °C for 90 min.); Lane 20 = λ DNA + AgNPs ((37 °C for 90 min.)) + Fenton's reagent (37 °C for 90 min.)

3.9.1 Antibacterial activity

AgNPs were found to be a strong inhibitor for *E. coli* with 1.00 mm and 1.75 mm diameter at 30 µl and 40 µl volume (Fig. 13B); for *S. aureus* zone of inhibition was 1.75 mm and 2.50 mm at 30 µl and 40 µl volume (Fig. 14B), while wells with rutin have 0.0 mm of diameter against both strains.

3.9.2 Cytotoxic assessment using MTT assay

The AgNPs depicted reducing the viability of 1×10^5 cells in a dose-dependent manner as per Fig. 15. The IC_{50} value of AgNPs is 785.37 ± 43.55 µg/ml.

4 Discussion

In this study, AgNPs were phyto-fabricated using rutin for potential biological activities. UV–visible spectroscopy is an expedient technique for the structural categorization of NPs [28]. Surface plasmon resonance (SPR) is the excellent optical property of metallic nanocomposites. It consists of an aggregate oscillation of electrons energized by the electromagnetic field of light. Thus, AgNPs are known to exhibit an intense surface plasmon absorption band in the range of 350-450 nm [29]. The records of zeta size are in accordance with Song and Kim [30] and Song and Kim [31]. An upsurge in NPs size is due to the effect of high $AgNO_3$ and/or reducing agent concentration, and successively it leads to the aggregation of particles [32]. Zeta potential study was executed for determining the stability and particle surface charge of AgNPs. The negative value clearly suggests the presence of strong electric charges on the particle surfaces to hinder future agglomeration and provides stability [33]. XRD is commonly employed to explore the characteristic and structural details like position, peak intensity, and width of the formed NPs [34]. The study result of XRD is in agreement with Supraja et al. [35], whereas in AFM analysis size of the AgNPs is found to be 47.29 nm [36]. As per Fig. 6, FESEM revealed a size between 80 and 85 nm. The aggregation of the AgNPs may be caused by components present on the NPs surface that acts as a capping agent [37]. FTIR spectroscopy served to categorize the biomolecules as per their functional group that not only capped but also helped in the reduction and stabilization during the synthesis process [38]. In the current study, AgNPs were observed with many functional groups, and Kubavat et al. [3] and Gaddala and Nataru [39] are also in agreement that AgNPs are capped by used reducing agents.

Ajitha et al. [21] prepared AgNPs using *Abrus precatorius* leaf extract and demonstrated UV–visible spectra at 420 nm, and crystallite size of 12 nm from XRD data. The AgNPs were spherical and aggregated with an average

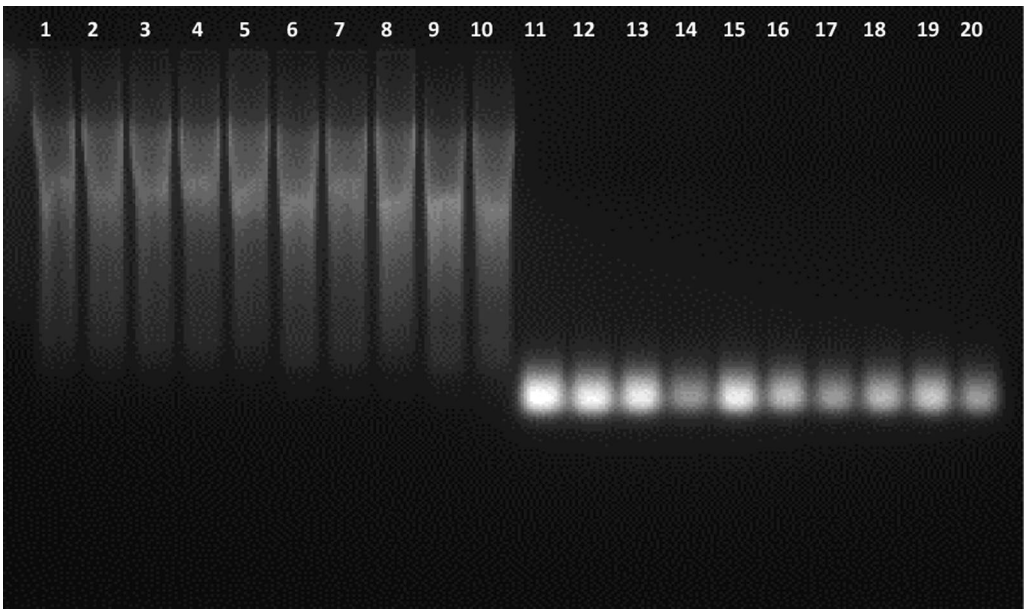

Fig. 12 Interaction of AgNPs with CT-DNA and HS-DNA. Lane 1 = Control CT-DNA; Lane 2 = CT-DNA + AgNPs (37 °C for 30 min.); Lane 3 = CT-DNA + Fenton's reagent (37 °C for 30 min.); Lane 4 = CT-DNA + AgNPs ((37 °C for 30 min.)) + Fenton's reagent (37 °C for 30 min.); Lane 5 = CT-DNA + AgNPs (37 °C for 60 min.); Lane 6 = CT-DNA + Fenton's reagent (37 °C for 60 min.); Lane 7 = CT-DNA + AgNPs ((37 °C for 60 min.)) + Fenton's reagent (37 °C for 60 min.); Lane 8 = CT-DNA + AgNPs (37 °C for 90 min.); Lane 9 = CT-DNA + Fenton's reagent (37 °C for 90 min.); Lane 10 = CT-DNA + AgNPs ((37 °C for 90 min.)) + Fenton's reagent (37 °C for 90 min.). Lane 11 = Control HS-DNA; Lane 12 = HS-DNA + AgNPs (37 °C for 30 min.); Lane 13 = HS-DNA + Fenton's reagent (37 °C for 30 min.); Lane 14 = HS-DNA + AgNPs ((37 °C for 30 min.)) + Fenton's reagent (37 °C for 30 min.); Lane 15 = HS-DNA + AgNPs (37 °C for 60 min.); Lane 16 = HS-DNA + Fenton's reagent (37 °C for 60 min.); Lane 17 = HS-DNA + AgNPs ((37 °C for 60 min.)) + Fenton's reagent (37 °C for 60 min.); Lane 18 = HS-DNA + AgNPs (37 °C for 90 min.); Lane 19 = HS-DNA + Fenton's reagent (37 °C for 90 min.); Lane 20 = HS-DNA + AgNPs ((37 °C for 90 min.)) + Fenton's reagent (37 °C for 90 min.)

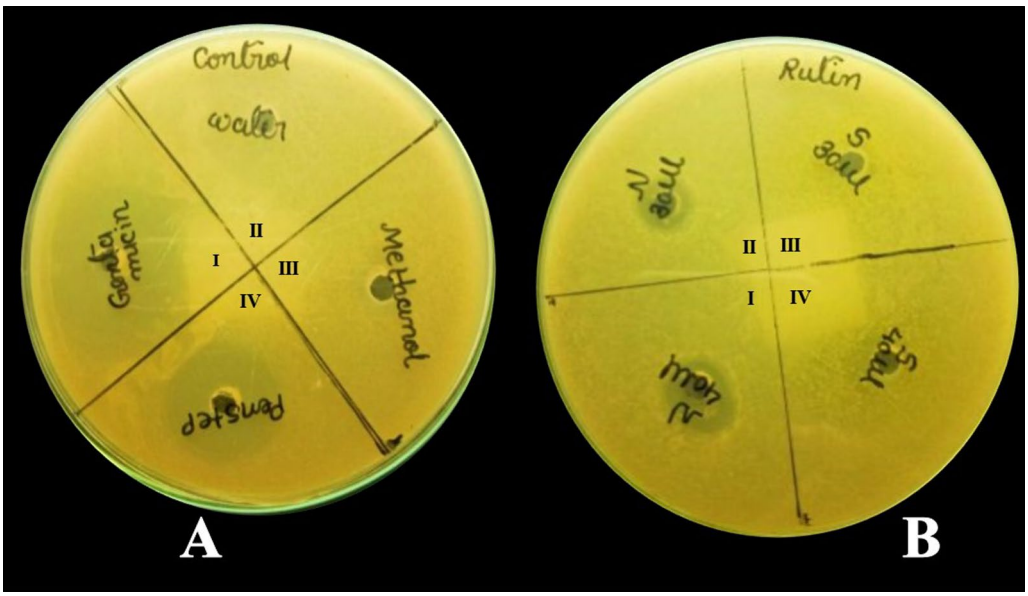

Fig. 13 Antibacterial activity against *E. coli*: Control: **AI**. Gentamicin, **AII**. DW, **AIII**. Methanol, **AIV**. PenStrep. **BI**. AgNPs (40 µl), **BII**. AgNPs (30 µl), **BIII**. Rutin (30 µl), **BIV**. Rutin (40 µl)

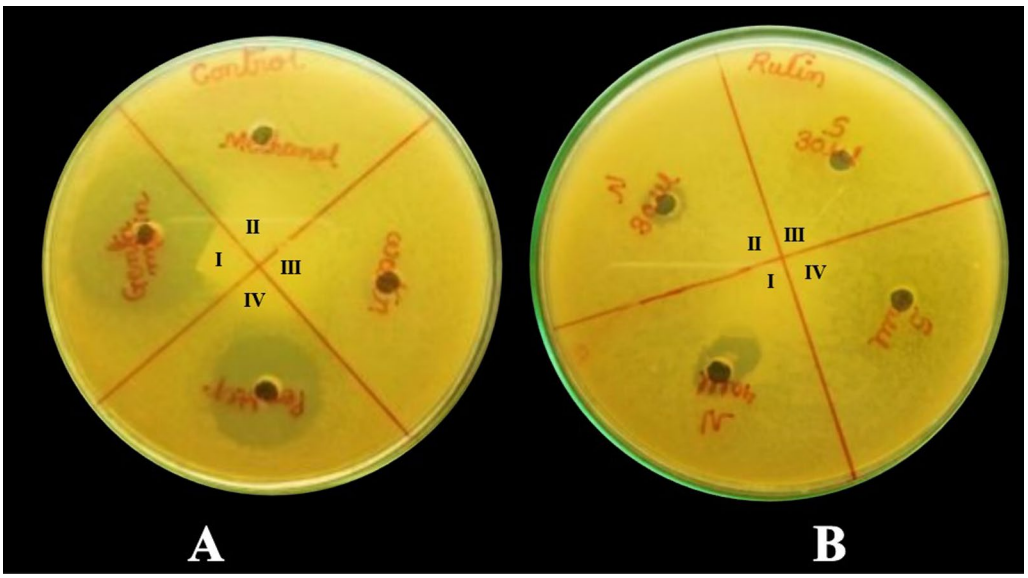

Fig. 14 Antibacterial activity against *S. aureus*: Control: **AI**. Gentamicin, **AII**. Methanol, **AIII**. DW, **AIV**. PenStrep **BI**. AgNPs (40 µl), **BII**. AgNPs (30 µl), **BIII**. Rutin (30 µl), **BIV**. Rutin (40 µl)

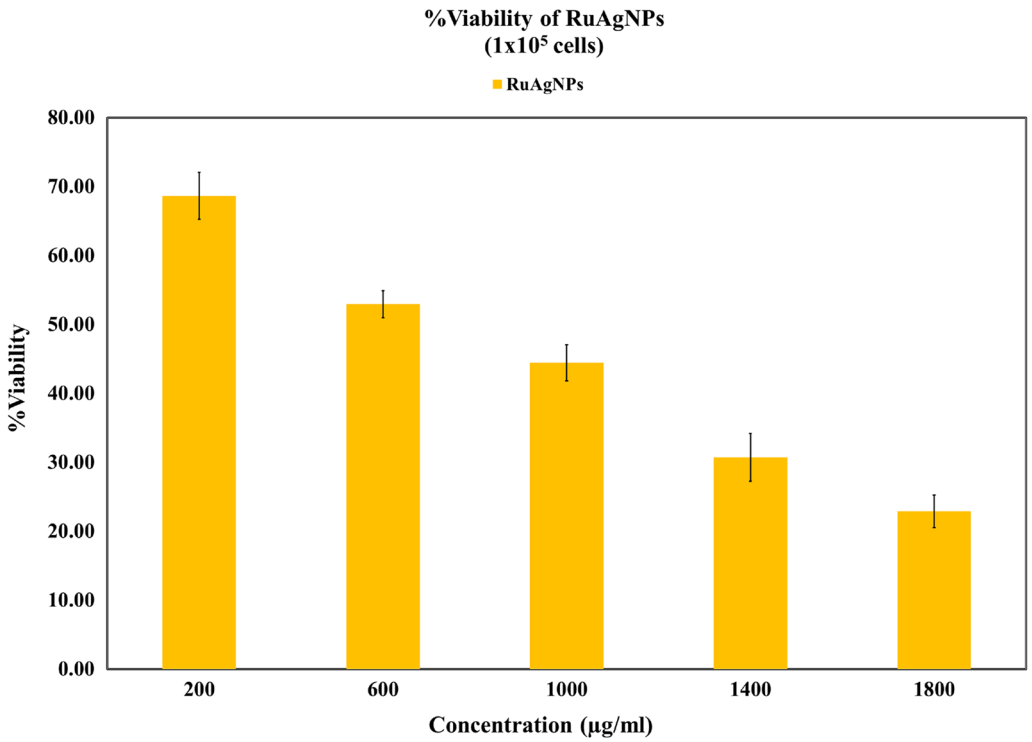

Fig. 15 Cytotoxic assessment of AgNPs using MTT assay

size of 20 nm in FESEM and FTIR spectra presented good peaks of different functional groups.

In the study by Zhou and Tang [40], the particle size of the AgNPs synthesized by quercetin and rutin was 3–22

and 4–17 nm, and the zeta potentials of the AgNPs were − 19.2 and − 20.5 mV, respectively, that showed negative charge ad good stability. Their XRD study demonstrated peaks at 38.3°, 44°, 64.6°, and 77.4°.

The role of compounds in the synthesis and capping of AgNPs has become clearer when antioxidant activities are measured [11]. DPPH radical is commonly used as the substrate to evaluate antioxidant activity. It is a stable free radical that can accept an electron to become a stable molecule (diphenylhydrazine). The scavenging ability was measured spectrophotometrically with a strong absorption band at 520 nm by changing the DPPH color from purple to yellow [41]. Figure 8 shows effective % inhibition, 86.95 ± 01.60% at 80 µg/ml by AgNPs, and Kubavat et al. [3] have mentioned good antioxidant power of *Abrus precatorius* Linn. and curcumin synthesized AgNPs using in vitro antioxidant assays like DPPH and PFRAP (potassium ferricyanide reducing power method). Prakash et al. [26] also found good antioxidant efficacy of biosynthesized AgNPs through $ABTS^{+}$ (Azino-bis-3-ethylbenzothiazoline-6-sulfonic acid) assay with an IC_{50} value of 462.56 µg/ml. UV–visible spectroscopy is the basic technique to study the stability of DNA and its interactions with small particles [23, 42, 43]. The study of AgNPs–DNA interactions was done by examining the changes in the absorption patterns. The spectrum of DNA shows maximum absorption at 260 nm due to chromophoric groups in purine and pyrimidine which are responsible for the electronic transitions. When NPs bind with DNA through intercalation normally results in hypochromism. Subsequently, the energy level of the π to π^* electron transition decreases, which causes a bathochromism (redshift). Hyperchromic shift is a result of DNA denaturation through electrostatic attraction between the compound/cations and DNA. A hypsochromic effect (blue shift) can be due to the unsuitable coupling of the π^*orbital of an intercalated ligand with the π orbital of the base pairs [44–48]. Kongor et al.[49] also reported hyperchromicity in the interaction of CPTH-AgNPs and CT-DNA. Reactive oxygen species (ROS) are the cause of oxidation in biomolecules leading to DNA and protein damage and consequently resulting in the occurrence of many free radical-induced maladies in humans [50]. Recently, the complexes that aim at the DNA have great importance in therapeutics [51]. It is known that DNA and NPs interact with each other by covalent bonds or adsorption [52] and antioxidant-capped AgNPs might help to reduce oxidative damage in DNA. In Figs. 11 and 12, synthesized AgNPs showed various interactions with studied DNA. A similar study was also done by Kongor et al. [53] with CPTH-AuNPs. It is also stated that the NPs show a genotoxic effect as their small size has high surface reactivity when compared with the mass structures [52]. AgNPs have a sustainable antibacterial effect against different pathogenic bacteria [54]. The subject of matter found that the AgNPs are promising and effective antibacterial agents against both *E. coli* and *S. aureus* bacteria. Taruna et al. [55] and Joseph et al. [56] also found the effective activity of AgNPs against various strains. In recent times, AgNPs with antibacterial activity are the most propagated and commercialized nanomaterial. However, AgNPs show high cytotoxicity toward both human and bacterial cells [57]. AgNPs have a significant contribution to human health, and thus, it is ought to be examined to encourage the downstream process.

5 Conclusion

In a nutshell, a simple, bioinspired, innocuous, and one-step process is employed for the synthesis of AgNPs by using the nutritive antioxidant rutin. The characteristic study reveals the emblematic shape, size, and potentiality of AgNPs enabling such green synthesized NPs applicable in various areas. Considerable clinical significance can be fulfilled by bioreduced AgNPs as they also possess remarkable antioxidant and antibacterial potential with subsequent cytotoxic assessment. The study results established that the synergy of AgNPs and the paradoxical genetic molecule, DNA, will aid in the selective delivery of desired analytes to the target through next-generation curative implements of NT. Moreover, the study is desired to explore the mechanism of biocapped AgNPs to cleave the DNA and a computational docking study is also required to investigate the dominant interactions of AgNPs with OMICs.

Abbreviations

°C: Celsius; µg: Microgram; µl: Microliter; µM: Micromolar; 2D: Two-dimension; 3D: Three-dimension; cm^{-1} M^{-1}: Reciprocal centimeter reciprocal meter; Hrs.: Hour; IC_{50}: Half maximal inhibitory concentration; M: Molar; min.: Minute; ml: Milliliter; mm: Millimeter; mM: Millimolar; mV: Millivolts; nm: Nanometer; PdI: Polydispersity index; PenStrep: Penicillin streptomycin; RPM: Rotation per minute; SE: Standard error; TAE: Tris acetic acid EDTA; UV–visible Spectroscopy: Ultraviolet–visible spectroscopy; V: Volt; λ-DNA: Lambda DNA.

Acknowledgements

The authors would like to thank Maliba Pharmacy College, Gujarat, India, where FTIR and Zeta sizer analysis were carried out, and Scientium Analyze Solutions, Jaipur, India, for XRD, AFM, and FESEM analysis. Pooja Trivedi would like to thank the Department of Science and Technology (DST), New Delhi, for providing the JRF-INSPIRE fellowship (IF190292). Manthan Panchal gratefully acknowledges the Human Resource Development Group-Council of Scientific & Industrial Research (CSIR), New Delhi, for Research Associate fellowship (File No. 09/070 (0064) 2019 EMR-I).

Author contributions
All authors have participated equally in this research and took the responsibility for the decision to submit for publication. All authors read and approved the final manuscript.

Funding
This research did not receive any specific grant.

Availability of data and materials
Not applicable.

Declarations

Ethics approval and consent to participate
Not applicable.

Consent for publication
Not applicable.

Competing interests
The authors declare no competing of interests.

Author details
[1]Department of Zoology, BMT, HGC and WBC, University School of Sciences, Gujarat University, Ahmedabad, India. [2]Department of Chemistry, University School of Sciences, Gujarat University, Ahmedabad, India. [3]Silver Oak Institute of Science, Silver Oak University, Ahmedabad, India.

Received: 12 April 2022 Accepted: 5 September 2022
Published online: 23 September 2022

References

1. Haq IU, Ijaz S, Khan NA (2020) Application of nanotechnology for integrated plant disease management. Plant Dis Manag Strateg Sustain Agric Tradi Mod Approach 13:173–185
2. Fouad DE, Zhang C, El-Didamony H, Yingnan L, Mekuria TD, Shah AH (2019) Improved size, morphology and crystallinity of hematite (α-Fe2O3) nanoparticles synthesized via the precipitation route using ferric sulfate precursor. Results Phys 12:1253–1261
3. Kubavat KK, Trivedi PG, Ansari HI, Sindhav GM (2019) Green molecule mediated synthesis of silver nanoparticles: antioxidant, antibacterial, cytotoxic and DNA interaction study. Chem Biol Interface 9(5):234–243
4. Kalpana D, Han JH, Park WS, Lee SM, Wahab R, Lee YS (2019) Green biosynthesis of silver nanoparticles using Torreya nucifera and their antibacterial activity. Arab J Chem 12(7):1722–1732
5. Sundarrajan S, Chandrasekaran AR, Ramakrishna S (2010) An update on nanomaterials-based textiles for protection and decontamination. J Am Ceram Soc 93(12):3955–3975
6. Thakkar KN, Mhatre SS, Parikh RY (2010) Biological synthesis of metallic nanoparticles. Nanomedicine 6(2):257–262
7. Parashar UK, Saxena PS, Srivastava A (2009) Bioinspired synthesis of silver nanoparticles. Dig J Nanomater Bios 4(1):159–166
8. Yaqoob AA, Umar K, Ibrahim MNM (2020) Silver nanoparticles: various methods of synthesis, size affecting factors and their potential applications–a review. Appl Nanosci 10(5):1369–1378
9. Emery L, Whelan S, Hirschi KD, Pittman JK (2012) Protein phylogenetic analysis of Ca2+/cation antiporters and insights into their evolution in plants. Front Plant Sci 3:1
10. Terenteva EA, Apyari VV, Dmitrienko SG, Zolotov YA (2015) Formation of plasmonic silver nanoparticles by flavonoid reduction: a comparative study and application for determination of these substances. Spectrochim Acta, Part A 151:89–95
11. Mittal AK, Kumar S, Banerjee UC (2014) Quercetin and gallic acid mediated synthesis of bimetallic (silver and selenium) nanoparticles and their antitumor and antimicrobial potential. J Colloid Interface Sci 431:194–199
12. Sundararajan B, Mahendran G, Thamaraiselvi R, Kumari BR (2016) Biological activities of synthesized silver nanoparticles from cardiospermum halicacabum L. Bull Mater Sci 39(2):423–431
13. Enogieru AB, Haylett W, Hiss DC, Bardien S, Ekpo OE. Rutin as a potent antioxidant: implications for neurodegenerative disorders. Oxid Med Cell Longev. 2018.
14. Kamalakkannan N, Prince PSM (2006) Antihyperglycaemic and antioxidant effect of Rutin, a polyphenolic flavonoid, in streptozotocin-induced diabetic wistar rats. Basic Clin Pharmacol Toxicol 98(1):97–103
15. An H, Jin B (2012) Prospects of nanoparticle–DNA binding and its implications in medical biotechnology. Biotechnol Adv 30(6):1721–1732
16. Shrivastava R, Kushwaha P, Bhutia YC, Flora SJS (2016) Oxidative stress following exposure to silver and gold nanoparticles in mice. Toxicol Ind Health 32(8):1391–1404
17. Selvamani S, Balamurugan S (2015) Phytochemical screening and GCMS analysis of acetone leaf extract of Acalypha indica (Linn.). Int J Res Stud Biosci 3(5):229–232
18. Khurana C, Vala AK, Andhariya N, Pandey OP, Chudasama B (2014) Antibacterial activity of silver: the role of hydrodynamic particle size at nanoscale. J Biomed Mater Res, Part A 102(10):3361–3368
19. Dwivedi AD, Gopal K (2010) Biosynthesis of silver and gold nanoparticles using Chenopodium album leaf extract. Colloids Surf, A 369(1–3):27–33
20. Weyermann J, Lochmann D, Zimmer A (2005) A practical note on the use of cytotoxicity assays. Int J Pharm 288(2):369–376
21. Ajitha B, Reddy YAK, Reddy PS (2014) Synthesis of silver nanoparticles: Green route, antimicrobial efficacy. Int J Curr Eng Technol 2:306–313
22. Blois MS (1958) Antioxidant determinations by the use of a stable free radical. Nature 181(4617):1199–1200
23. Rahban M, Divsalar A, Saboury AA, Golestani A (2010) Nanotoxicity and spectroscopy studies of silver nanoparticle: calf thymus DNA and K562 as targets. J Phys Chem 114(13):5798–5803
24. Lee SE, Ju EM, Kim JH (2002) Antioxidant activity of extracts from Euryale ferox seed. Exp Mol Med 34(2):100–106
25. Mosmann T (1983) Rapid colorimetric assay for cellular growth and survival: application to proliferation and cytotoxicity assays. J Immunol Methods 65(1–2):55–63
26. Prakash J, Shekhar H, Yadav SR, Dwivedy AK, Patel VK, Tiwari S, Vishwakarma NK (2021) Green synthesis of silver nanoparticles using Eranthemum Pulchellum (Blue Sage) aqueous leaves extract: Characterization, evaluation of antifungal and antioxidant properties. Biomed Biotechnol Res J (BBRJ) 5(2):222–228
27. Hooresfand Z, Ghanbarzadeh S, Hamishehkar H (2015) Preparation and characterization of rutin-loaded nanophytosomes. Pharm Sci 21(3):145–151
28. Nayagam V, Gabriel M, Palanisamy K (2018) Green synthesis of silver nanoparticles mediated by Coccinia grandis and Phyllanthus emblica: a comparative comprehension. Appl Nanosci 8(3):205–219
29. Jayandran M, Haneefa MM, Balasubramanian V (2015) Green synthesis and characterization of manganese nanoparticles using natural plant extracts and its evaluation of antimicrobial activity. J Pharm Sci 5(12):105–110
30. Song JY, Kim BS (2009) Rapid biological synthesis of silver nanoparticles using plant leaf extracts. Bioprocess Biosyst Eng 32(1):79–84
31. Song JY, Kim BS (2008) Biological synthesis of bimetallic Au/Ag nanoparticles using Persimmon (Diopyros kaki) leaf extract. Korean J Chem Eng 25(4):808–811
32. Ali M, Kim B, Belfield KD, Norman D, Brennan M, Ali GS (2016) Green synthesis and characterization of silver nanoparticles using Artemisia absinthium aqueous extract-a comprehensive study. Mater Sci Eng C 58:359–365
33. Anandalakshmi KJ, Ramasamy V (2016) Characterization of silver nanoparticles by green synthesis method using Pedalium murex leaf extract and their antibacterial activity. Appl Nanosci 6(3):399–408
34. El-Saadony MT, El-Wafai NA, El-Fattah HIA, Mahgoub SA (2019) Biosynthesis, optimization and characterization of silver nanoparticles using a soil isolate of Bacillus pseudomycoides MT32 and their antifungal activity against some pathogenic fungi. Adv Anim Vet Sci 7(4):238–249
35. Supraja N, Prasad TNVKV, David E, Krishna TG (2016) Antimicrobial kinetics of Alstonia scholaris bark extract-mediated AgNPs. Appl Nanosci 6(5):779–787
36. Moosa A, Ridha AM, Allawi MH (2015) Green synthesis of silver nanoparticles using spent tea leaves extract with atomic force microscopy. Int J Curr Eng Technol 5(5):3233–3241

37. Vanaja M, Annadurai G (2013) Coleus aromaticus leaf extract mediated synthesis of silver nanoparticles and its bactericidal activity. Appl Nanosci 3(3):217–223
38. Shaik MR, Khan M, Kuniyil M, Al-Warthan A, Alkhathlan HZ, Siddiqui MRH, Shaik JP, Ahamed A, Mahmood A, Khan M, Adil SF (2018) Plant-extract-assisted green synthesis of silver nanoparticles using Origanum vulgare L. extract and their microbicidal activities. Sustainability 10(4):913
39. Gaddala B, Nataru S (2015) Synthesis, characterization and evaluation of silver nanoparticles through leaves of Abrus precatorius L.: an important medicinal plant. Appl Nanosci 5(1):99–104
40. Zhou Y, Tang RC (2018) Facile and eco-friendly fabrication of colored and bioactive silk materials using silver nanoparticles synthesized by two flavonoids. Polymers 10(4):404
41. Salar RK, Sharma P, Kumar N (2015) Enhanced antibacterial activity of streptomycin against some human pathogens using green synthesized silver nanoparticles. Resour Effic Technol 1(2):106–115
42. Dehkordi MF, Dehghan G, Mahdavi M, Feizi MAH (2015) Multispectral studies of DNA binding, antioxidant and cytotoxic activities of a new pyranochromene derivative. Spectrochim Acta A Mol Biomol Spectrosc 145:353–359
43. Roy S, Sadhukhan R, Ghosh U, Das TK (2015) Interaction studies between biosynthesized silver nanoparticle with calf thymus DNA and cytotoxicity of silver nanoparticles. Spectrochim Acta A Mol Biomol Spectrosc 141:176–184
44. Kaushal R, Thakur S, Nehra K (2016) Ct-DNA binding and antibacterial activity of octahedral titanium (IV) heteroleptic (benzoylacetone and hydroxamic acids) complexes. Int J Med Chem 16:1–11
45. Sirajuddin M, Ali S, Badshah A (2013) Drug–DNA interactions and their study by UV–Visible, fluorescence spectroscopies and cyclic voltammetry. J Photochem Photobiol B 124:1–19
46. Arshad N, Abbas N, Bhatti MH, Rashid N, Tahir MN, Saleem S, Mirza B (2012) Synthesis, crystal structure, DNA binding and in vitro biological studies of Ni (II), Cu (II) and Zn (II) complexes of N-phthaloylglycine. J Photochem Photobiol B 117:228–239
47. Ribeiro APC, Anbu S, Alegria ECBA, Fernandes AR, Baptista PV, Mendes R, Matias AS, Mendes M, da Silva MG, Pombeiro AJL (2018) Evaluation of cell toxicity and DNA and protein binding of green synthesized silver nanoparticles. Biomed Pharmacother 101:137–144
48. Hegde AH, Prashanth SN, Seetharamappa J (2012) Interaction of antioxidant flavonoids with calf thymus DNA analyzed by spectroscopic and electrochemical methods. J Pharm Biomed Anal 63:40–46
49. Kongor A, Panchal M, Athar M, Jha PC, Jhala D, Sindhav G, Shah N, Jain VK (2018) Selective fluorescence sensing of Cu (II) ions using calix [4] pyrrole fabricated Ag nanoparticles: a spectroscopic and computational approach. J Mol Liq 269:467–475
50. Sharma N, Bhardwaj R, Kumar S, Kaur S (2011) Evaluation of Bauhinia variegata L. bark fractions for in vitro antioxidant potential and protective effect against H2O2-induced oxidative damage to pBR322 DNA. Afr J Pharm Pharmacol 5(12):1494–1500
51. Aygün A, Özdemir S, Gülcan M, Cellat K, Şen F (2020) Synthesis and characterization of Reishi mushroom-mediated green synthesis of silver nanoparticles for the biochemical applications. J Pharm Biomed Anal 178:112970
52. Koca FD, Duman F (2019) Genotoxic and cytotoxic activity of green synthesized TiO2 nanoparticles. Appl Nanosci 9(5):815–823
53. Kongor A, Panchal M, Athar M, Makwana B, Sindhav G, Jha PC, Jain V (2018) Synthesis and modeling of calix [4] pyrrole wrapped Au nanoprobe for specific detection of Pb (II): Antioxidant and radical scavenging efficiencies. J Photochem Photobiol, A 364:801–810
54. Morones JR, Elechiguerra JL, Camacho A, Holt K, Kouri JB, Ramírez JT, Yacaman MJ (2005) The bactericidal effect of silver nanoparticles. Nanotechnology 16(10):2346
55. Taruna KJ, Bhatti J, Kumar P (2016) Green synthesis and physico-chemical study of silver nanoparticles extracted from a natural source Luffa acutangula. J Mol Liq 224:991–998
56. Joseph J, Deborah KS, Raghavi R, Shamya AM, Aruni W (2021) Green synthesis of silver nanoparticles using Phyllanthus amarus Seeds and their antibacterial activity assessment. Biomed Biotechnol Res J (BBRJ) 5(1):35–38
57. Banasiuk R, Krychowiak M, Swigon D, Tomaszewicz W, Michalak A, Chylewska A, Ziabka M, Lapinski M, Koscielska B, Narajczyk M, Krolicka A (2020) Carnivorous plants used for green synthesis of silver nanoparticles with broad-spectrum antimicrobial activity. Arab J Chem 3(1):1415–1428

Publisher's Note